ELSEVIER

Polymer 42 (2001) 6723–6731

polymer

www.elsevier.nl/locate/polymer

Structure development and crystallization behaviour of PP/nanoparticulate composite

C. Saujanya, S. Radhakrishnan*

Polymer Science and Engineering, National Chemical Laboratory, Council of Science and Industrial Research, Pune 411008, India

Received 20 November 2000; received in revised form 9 January 2001; accepted 31 January 2001

Abstract

The structure development and crystallization behaviour of polypropylene (PP) containing nanoparticles of calcium phosphate prepared by a new route based on matrix mediated control of growth and morphology was investigated by X-ray diffraction (XRD), optical microscopy and DSC techniques. The results obtained were compared with that of PP containing conventionally prepared calcium phosphate (CaP0). Both nanoparticle filled PP as well as CaP0 filled PP crystallized in monoclinic α crystalline phase. However, considerable changes were observed in the relative intensities of the XRD peaks, especially the peak II (040 reflection), in the case of PP filled with nanosize calcium phosphate. The isothermal crystallization curves showed dramatic increase of crystallization rate and decrease in $t_{1/2}$ value for PP/nanoparticulate composites resulting in a rapid decrease in the ultimate spherulite size as compared to PP/CaP0 samples. The nucleating efficiency was found to be dependent on the particle size as inverse exponential power law. These results were further confirmed by DSC analysis. The optical transparency of the PP/nanoparticle composites was found to be much higher than that containing conventional CaP0 for the same concentrations and this could be associated with the reduction in the PP crystallite size.

Keywords: Nanoparticles; Calcium phosphate; Nanocomposite

1. Introduction

Polymer nanocomposites comprise a new class of materials where nanoscale particulates (inorganic such as clay or any other mineral) are finely dispersed within a matrix. These have been reported to exhibit markedly improved properties as compared to the pure polymers or conventional particulate composites [1–5]. These include increase of modulus and strength, improved barrier properties, increase in solvent and heat resistance, good optical transparency, etc. Further, these improvements are achieved at very low loadings of the inorganic component (1–10 wt%) as compared to conventional filled polymers, which require a high loading of the order of 25–40 wt%.

Many routes have been attempted in recent years for the synthesis of inorganic/organic nanocomposites. These include mainly (a) sol–gel processing [6,7], (b) in situ intercalative polymerization [8,9], and (c) in situ polymerization [10,11], etc. Polymer/clay nanocomposites have been extensively studied by using both in situ intercalative and polymerization methods. These were investigated by dispersing the mineral clays in various polymer matrices such as nylon-6 [12], polypropylene [13] (PP), polyethylene terephthalate [14], polystyrene [15], epoxy [16], polyacrylates [17,18], etc. A large improvement in the properties of the polymers was observed for such materials. However, the above routes employed by the various researchers showed a major disadvantage of difficulty in handling and processing of nanoparticles. Further, in the case of semicrystalline polymers, it is known that the crystallization behaviour and morphology get affected by the presence of particulate additives especially at low concentrations. These structural features can affect the overall properties of the material but such detailed investigations have not been reported earlier.

Matrix mediated control of growth and morphology has received considerable attention in the recent years since it offers a novel route to material synthesis [19–21]. This novel route was earlier investigated by us in different types of materials such as $CaCO_3$, K_2CO_3, CdS, $CaSO_4$, etc. which were prepared in situ within a polymer matrix such as polyethylene oxide (PEO) giving rise to modification of morphology, crystalline phase, orientation and growth habits of these compounds [22–24]. This method

* Corresponding author. Tel.: +91-212-331-453; fax: +91-020-589-3041.

E-mail address: srr@ems.ncl.res.in (S. Radhakrishnan).

0032-3861/01/$ - see front matter
PII: S0032-3861(01)00140-9

presents various advantages over the conventional methods mentioned above since (a) it is a simple precipitation technique, which can be carried out at room temperature; (b) it is easy to handle and process the powders; and (c) it leads to control of the overall morphology, uniformity of size and dispersion, etc. In the present investigation, we have employed this novel method for the preparation of nanosize particles of calcium phosphate (CaP) [25] which were further dispersed in a polymer matrix such as PP. This additive was chosen since it is expected to improve the flame resistance of the polymer.

The main aim of the present investigations was to study the effect of nanosize calcium phosphate filler particles on the structure development and crystallization behaviour of PP and compare the same with conventionally prepared calcium phosphate.

2. Experimental

The nanosized calcium phosphate filler particles were synthesized using in situ deposition technique in presence of PEO (CaPI) as follows: Firstly, a complex of calcium chloride with PEO was prepared in desired proportions in methanol. An appropriate stoichiometric amount of trisodium phosphate in distilled water was added to the above complex slowly without stirring. The whole mixture was allowed to digest at room temperature for 20 h when both the chloride and phosphate ions diffused through the PEO and formed a white gel like precipitate, which was filtered, washed and dried. The concentrations of PEO–$CaCl_2$ complex were varied in the range from 2:1, 4:1, 8:1, 16:1 and 32:1, respectively.

In another set of experiments, the nanosized filler particles were prepared in situ using a blending technique (CaPII) which gave further reduction in particle size. The initial procedure of formation of PEO–$CaCl_2$ complex in methanol was the same as described above except that after the formation of complex, it was blended by mixing it with amorphous polymer such as polyvinyl acetate (PVAc) solution (dissolved in methanol) after which it was allowed to stabilize over a period of 10 h. The composition of the blend was varied from 20 to 80% PVAc in PEO/PVAc blends. An appropriate stoichiometric amount of trisodium phosphate in distilled water was then added to the above blended complex slowly without stirring and the whole mixture was digested and the precipitate filtered, washed and dried in the same manner as described above. These two grades were compared with that of calcium phosphate prepared without any polymer (CaP0). The crystal structure and particle size were investigated by X-ray diffraction (XRD) and TEM techniques in the same manner as described elsewhere [26,27].

In order to study the crystallization behaviour of PP filled with calcium phosphate nano-particles, the composite was prepared by taking desired quantity of all three types of filler (CaP I, II, O) with respect to PP powder (Indothane, SM85N, MFI 8-12, IPCL, India) in an agate pestle and mortar. The composition of filler was varied from 2, 5 and 10 wt% with respect to PP. A small quantity of the mixed powder was isothermally melt crystallized on the hot stage of the microscope at 115°C. It was also compression molded in a single ended die at 29 MPa pressure for 30 s to form thin discs (12 mm diameter, 2 mm thickness) which were subsequently subjected to the melt crystallization on the hot stage (melt temp. = 190°C, crystallization T_c at 115°C, time = 20 min). The crystallization behaviour was investigated by recording the growth of spherulites as well as the intensity (grey scale) of transmitted light in the cross polar mode of the optical polarizing microscope (Leitz, Germany) coupled to the image analyzer system (VIDPRO 32, Leading Edge, Australia). The structure development and morphology were investigated by XRD and optical microscopy in the same manner as reported elsewhere [28,29]. The DSC thermograms were recorded on Perkin–Elmer instrument for a few of the PP/CaPI nano sized samples in order to determine the peak crystallization temperature T_c and melting point T_m as compared to pure PP. The optical transparency of PP nanocomposites was obtained from the absorption spectra in the visible range obtained on Shimadzu UV–Vis spectrophotometer.

3. Results and discussion

Fig. 1 shows the XRD scans for calcium phosphate synthesized in PEO alone (CaPI) represented by the curves B to F with increasing concentration of the polymer and curve A corresponds to that prepared without any polymer. There are a number of crystalline forms reported for calcium

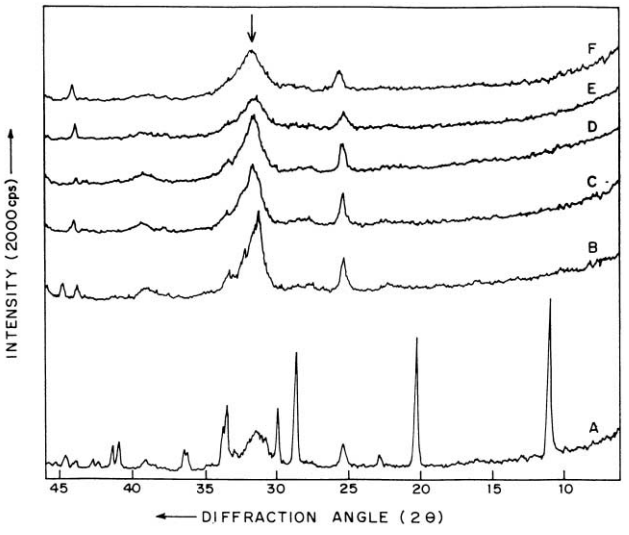

Fig. 1. XRD scans for calcium phosphate synthesized in situ PEO (CaPI): curves B to F represent increasing level of polymer in the starting complex 2:1, 4:1, 8:1, 16:1 and 32:1, respectively, while curve A that prepared without any polymer (conventional method CaP0).

phosphate existing in both anhydrous and hydrated states. The detailed analysis of XRD is given in Table 1. From the XRD analysis, it can be observed that calcium phosphate prepared without polymer (CaP0, curve A) is composed of mixed phase of calcium orthophosphate dihydrate (major) and β-calcium orthophosphate (minor phase). In presence of PEO (CaPI, curves B to F) a drastic change in the diffraction pattern is observed with a number of peaks suppressed compared to curve A. The detailed analysis of various peaks (see Table 1) shows the exclusive formation of β-calcium orthophosphate. It is also interesting to note that with the increase of PEO concentration from curves B to F, the XRD peaks broadens ($2\theta = 31.5°$). The extent of broadening shows small size of crystals, which could be

Table 1
XRD analysis of calcium phosphate synthesized by normal precipitation route (CaP0). (Reference: ASTM Diffraction Data Files 3-0690-91 (1950), 1-0395 (1950))

D (obs)	d (rep)	I/I_0	Assignment
7.89	7.6	100	Calcium orthophosphate dihydrate
4.29	4.24	83	Calcium orthophosphate dihydrate
3.49	3.40	18	β calcium orthophosphate
3.10	3.04	75	β calcium orthophosphate, calcium orthophosphate dihydrate
2.98	2.93	41	Calcium orthophosphate dihydrate
2.84	2.89	28	β calcium orthophosphate
2.78	2.75	17	β calcium orthophosphate
2.75	2.70	16	β calcium orthophosphate
2.66	2.62	42	Calcium orthophosphate dihydrate
2.64	2.60	29	β calcium orthophosphate
2.47	2.52	12	β calcium orthophosphate
2.45	2.40	16	β calcium orthophosphate, calcium orthophosphate dihydrate
2.29	2.26	8	β calcium orthophosphate, calcium orthophosphate dihydrate
2.19	2.16	18	Calcium orthophosphate dihydrate
2.11	2.08	8	Calcium orthophosphate dihydrate
2.05	2.06	5	β calcium orthophosphate
2.02	2.02	8	β calcium orthophosphate, calcium orthophosphate dihydrate
1.97	1.93	7	β calcium orthophosphate
1.90	1.88	14	β calcium orthophosphate, calcium orthophosphate dihydrate
1.87	1.82	9	β calcium orthophosphate, calcium orthophosphate dihydrate
1.84	1.78	22	β calcium orthophosphate, calcium orthophosphate dihydrate

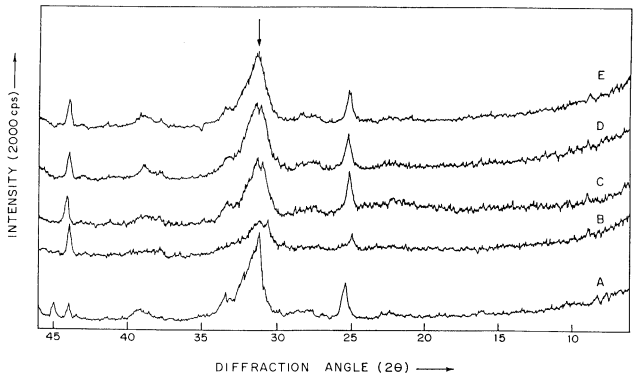

Fig. 2. XRD scans for calcium phosphate synthesized using PEO/PVAc blends (CaPII). Curve A corresponds to that prepared in PEO only while curves B to E correspond to PEO/PVAc blend with PVAc concentration of 80, 60, 40 and 20 wt%, respectively.

associated due to good molecular mixing. Thus a strong influence of polymer matrix on the structure and growth behaviour of calcium phosphate crystals is clearly seen in these data. Since calcium chloride is first complexed with PEO, the calcium atoms are strongly held within the polymer chains. The growth of subsequent formation of calcium phosphate crystals is therefore restricted to only certain crystalline phase as compared to large number of phases developed in normal solution precipitation.

The most striking feature of the present work can be observed in Fig. 2, which shows the XRD scans for calcium phosphate synthesized in PEO/PVAc blends (CaPII). The curve A corresponds to calcium phosphate prepared in PEO only while curves B, C, D and E correspond to that prepared in PEO/PVAc blends with PVAc concentration of 80, 60, 40 and 20%, respectively. The formation of exclusively single phase of β-calcium orthophosphate is seen even in this case. It is interesting to note that the peak intensity in curve A (PEO alone) at 2θ of 31.5° is quite sharp or in other words less broad as compared to curves B to E, respectively. Also, curve B shows greater broadening of the peak and it decreases with increase of PEO concentration (decrease of PVAc) from 20 to 80%. As the broadening of the peak corresponds to small crystallite size, it can be observed that with increase of PVAc concentration in the blend, the crystallite size reduces much more as compared to curve A.

The particle/crystallite size was estimated from full width at half maxima of the XRD peak (marked by arrow in Figs. 1 and 2 at $2\theta = 31.5°$ using Scherrer's formula [30,31] and the results are given in Table 2. Table 2 shows the particle size analysis of calcium phosphate prepared in presence of PEO alone (CaPI) of Fig. 1. It can be seen from the table that the calcium phosphate prepared without any polymer (CaP0) has an average particle size of 82 nm while that in presence of PEO alone (CaPI) causes lowering of particle size. In other words, with the increase in the concentration of PEO, (from 2:1 to 32:1 PEO–$CaCl_2$ complex) there is a

Table 2
Particle size analysis of calcium phosphate

Composition	Crystallite size (L)[a] (nm)
Prepared in PEO alone (CaPI)	
CaP(0)	82
2:1 PEO-complex	12
4:1 PEO-complex	9
8:1 PEO-complex	9
16:1PEO-complex	8
32:1 PEO-complex	7
Prepared by blending method using 8:1 PEO-complex (CaPII)	
PEO/PVAc (100:0)	9
PEO/PVAc (80:20)	7.5
PEO/PVAc (60:40)	7
PEO/PVAc (20:80)	5

[a] Determined from Scherrer's formula.

reduction in the particle size and it drops to as low as 7 nm at 32:1 PEO complex. Table 2 shows the particle size analysis of the calcium phosphate obtained by the blending technique (Fig. 2) for 8:1 PEO complex. The calcium phosphate prepared in the presence of PEO alone shows a particle size of 9 nm while in presence of blends with increase of PVAc concentration, it reduces further down to few nm levels, i.e. as low as 5 nm. This lowering of particle size in case of blends as compared to PEO alone can be explained as follows: The complex PEO/$CaCl_2$ is immiscible with PVAc and as the composition becomes PVAc rich, the domain size of the dispersed phase (PEO complex) is very small. The calcium phosphate formation during subsequent reaction is then restricted within such domains leading to drastic reduction in their particle size.

Fig. 3a shows the TEM micrograph of calcium phosphate crystals in PEO/PVAc (60/40) blend and Fig. 3b represents the selected area electron diffraction pattern recorded at an accelerated voltage of 100 kV. The sample shows the average particle size of less than 10 nm. Higher magnifications were attempted but the images were unstable and diffused due to the damage of the polymer matrix caused by high-accelerated electron beam voltage impinging on the same. The detailed analysis of selected area diffraction results reveals β-calcium orthophosphate having

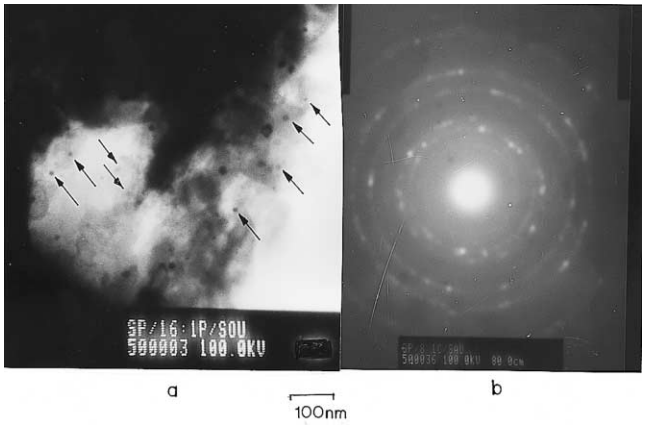

Fig. 3. (a)TEM micrograph of calcium phosphate crystals (CaPII) in PEO/PVAc (60/40) blend (the arrows indicate the particles), (b) represents the selected area electron diffraction pattern recorded at an accelerated voltage of 100 kV. Magnification 100 K.

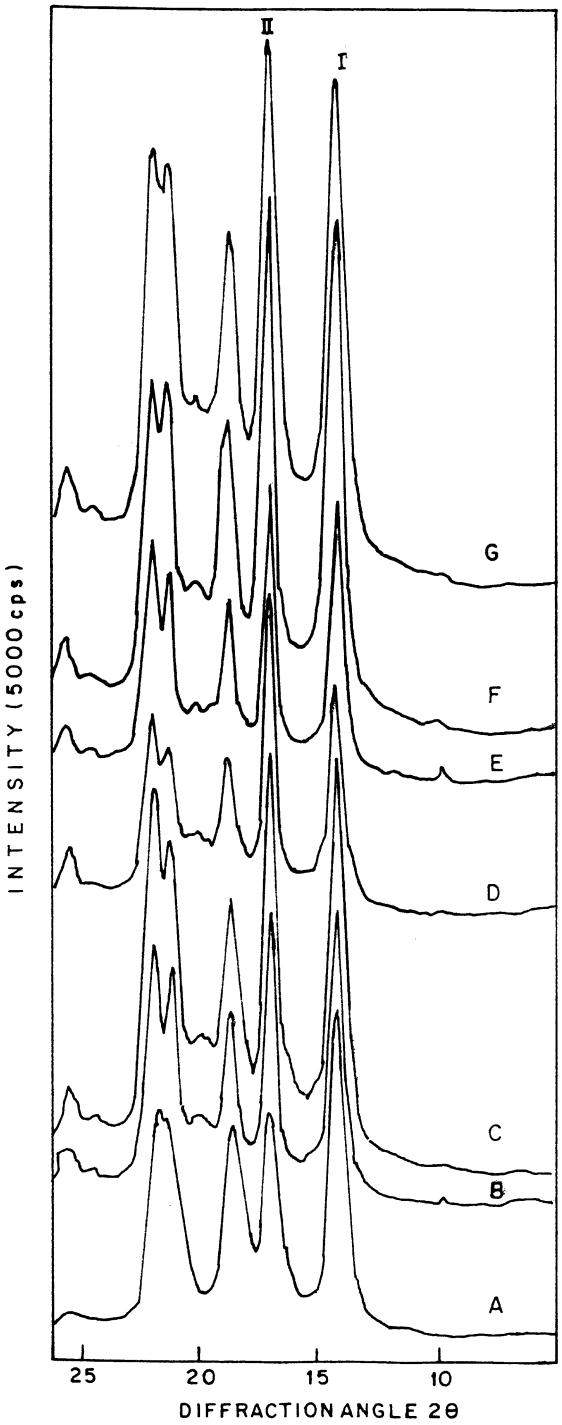

Fig. 4. XRD scans for PP/$Ca_3(PO_4)_2$ samples melt crystallized at 115°C. Curve A: pure PP, Curve B: PP/CaP0 while curves C to G correspond to calcium phosphate (CaPI) prepared in presence of increasing concentration of PEO mentioned in Fig. 1.

monoclinic crystalline structure, which is in good agreement with the structure obtained from the XRD data. There is some aggregation of the particles seen which can be during the precipitation process when the polymer itself forms agglomerates otherwise the particles are well dispersed. These results are consistent with the result described above for XRD data.

Fig. 4 shows the WAXD scans for PP-calcium phosphate particulate composite samples melt crystallized at 115°C. Curve A corresponds to pure PP and curve B that of conventionally prepared calcium phosphate (PP/CaP0) while curves C to G correspond to calcium phosphate prepared in presence of increasing concentration of PEO (CaPI), respectively. Pure PP (without any filler) shows five prominent peaks in the 2θ range of 10–30°, which correspond to monoclinic α crystalline phase. In the case of PP with CaP0 as well as nanoparticle filled PP (PP/CaPI) same numbers of peaks are observed in this range of 2θ, which suggests that these also contain mainly α-phase. However, the difference lies in the relative intensities of the peaks, especially the intensity of peak II, which change considerably in the presence of nanoparticles. It is interesting to note that the intensity of peak II increases with an increase in the concentration of PEO (curve C–G). The variation of the intensity of the peak II (040 reflection of α phase of PP) with respect to first peak ($2\theta = 14°$, 110 reflection of α phase of PP) was determined from the XRD and the results are presented in Table 3 as a function of particle size. It is obvious that the peak II for PP/CaP0 is nearly equal to peak I at a high particle size of 82 nm whereas for PP/CaPI it increases with a decrease of particle size. This increase in the intensity of peak II in the latter case can be due to small particle size or nanoparticles of CaP formed with increasing concentration of PEO which suggests high nucleation efficiency of CaP nanoparticles on the structure of PP. As the peak II corresponds to (040) reflection of α form of PP, it can be concluded that there is a preferential growth of PP crystallites along the *b*-axis during nucleation.

Fig. 5 shows the WAXD scans for PP/calcium phosphate prepared by blending technique for 8:1 PEO complex. Curve A corresponds to XRD patterns of PP/CaP0 and curve B that of PP/CaPI. Curves C and D correspond to PP/CaPII with increasing concentration of PVAc. On comparing the graphs, it is found that even in case of blends, the XRD pattern of PP filled with nanoparticles of calcium phosphate crystallizes in monoclinic α phase. However, there is a remarkable change in the intensity of peak II with increase in the concentration of PVAc (curves C and D) as compared to curves A and B. Table 3 shows the variation of intensity of peak II with respect to first peak as described earlier for all the curves as a function of 1/particle size. From the data, it can be surmised that peak II intensity increases as the particle size reduces. This occurs when the concentration of PVAc is higher in case of blends

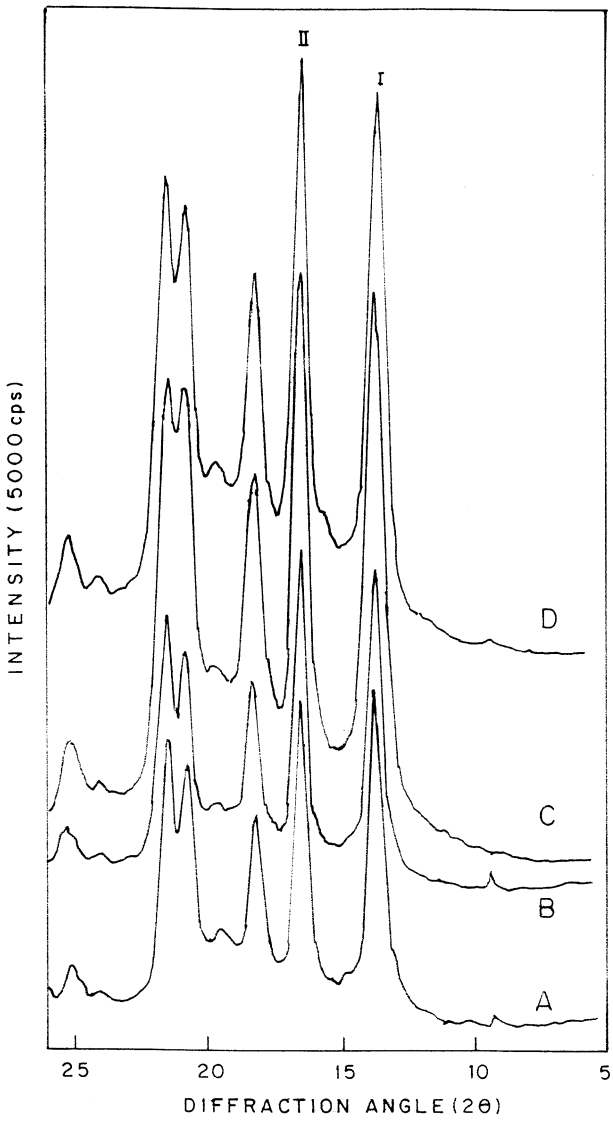

Fig. 5. Comparison of XRD scans of PP/CaP samples melt crystallized at $T_c = 115$°C with different particle size of additive. Curves A to D correspond to particle size of 82, 9, 7.5 and 7 nm, respectively.

Table 3
Intensity ratio of XRD peaks (PII/PI) as a function of particle size of calcium phosphate

Composition	Intensity ratio	Particle size (nm)
In PEO (CaPI)		
CaP(0)	0.979	82
2:1 (PEO-complex)	0.992	12
4:1 (PEO-complex)	1.370	9
8:1 (PEO-complex)	1.063	9
16:1(PEO-complex)	1.047	8
32:1(PEO-complex)	1.172	7
Prepared from blends (CaPII) using 8:1 PEO-complex (CaPII)		
CaP(0)	0.979	82
PEO/PVAc (100:0)	1.063	9
PEO/PVAc (80:20)	1.030	7.5
PEO/PVAc (60:40)	1.066	7

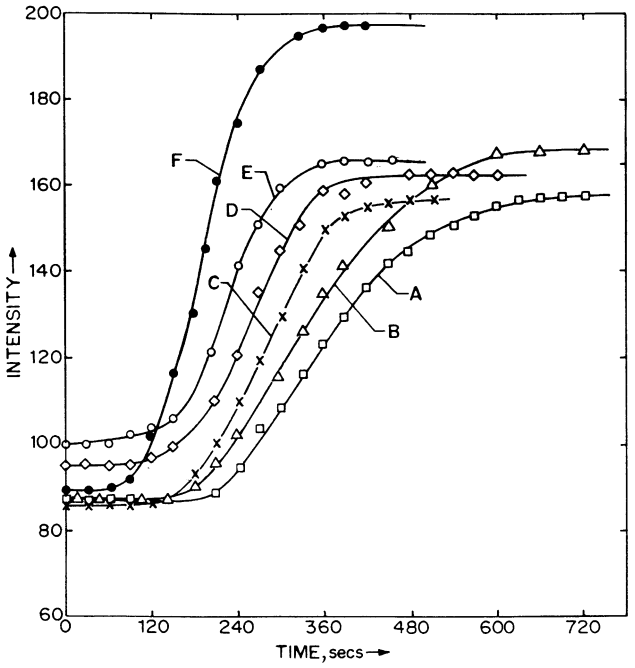

Fig. 6. Isothermal crystallization curves represented as transmitted intensity as a function of time at $T_c = 115°C$ for PP/CaP samples containing 2 wt% filler concentration. Curves A to F correspond to particle size of 82, 12, 9, 9, 8 and 7 nm, respectively.

as compared to curves A and B. This high intensity of peak II as explained earlier can be correlated to the decrease of particle size of calcium phosphate which drops further down in presence of high PVAc content and hence shows stronger nucleating effect as compared to that observed in PEO alone.

The crystallization behaviour of PP filled with nanoparticles of calcium phosphate in presence of PEO alone (CaPI) were studied and the results were compared with that prepared without any polymer (PP/CaP0). It was studied by plotting a graph of transmitted light intensity as a function of time at $T_c = 115°C$. Fig. 6 shows the plots for PP with 2 wt% filler concentration. Curves B, C, D and E in figure correspond to calcium phosphate filled with increasing concentration of PEO while curve A corresponds to calcium phosphate without any polymer. On comparing the graphs, it can be seen that with increase of PEO concentration from curves B to F, the induction period becomes much smaller with faster crystallization curves than curve A. From these curves, the crystallization half times ($t_{1/2}$) and the crystallization rates (slope) were determined which are represented in Table 4 as a function of particle size. It is evident from the table that when the particle size becomes smaller, the $t_{1/2}$ value decreases and at a particle size of 8 nm, the $t_{1/2}$ value is as low as 204 s for 2 wt% filler concentration. Similarly, the growth rates are also higher with a maximum growth rate of 0.66 at 8 nm particle size. Thus a drastic reduction in $t_{1/2}$ value and high growth rates are observed together with decrease of ultimate spherulite size for 2 wt% filler concentration in case of PP/CaPI compared to PP/CaP0. This clearly brings out the role of smaller particle size of calcium phosphate (of the order of few nm levels) on the crystallization of PP. From these various findings it can be observed that although calcium phosphate prepared without any polymer nucleates PP, the nanosize calcium phosphate prepared by in situ technique (PEO) shows much greater nucleation efficiency on the structure of PP. This strong nucleation efficiency of PP in the latter case is due to a very high active surface area enabled by the nanoparticles during nucleation, which in turn gives rise to faster crystallization rates of PP.

Table 4
Variation of $t_{1/2}$ value and crystallization rates (slope) with particle size of filler at concentration of 2 wt% (CaPI)

Composition 2 wt%	$t_{1/2}$	Particle size (nm)
(a) $t_{1/2}$ values		
CaP(0)	361	82
2:1 PEO-complex	327	12
4:1 PEO-complex	263	9
8:1 PEO-complex	206	9
16:1PEO-complex	204	8
(b) *Crystallization rates*		
	Rate (μm/s)	Particle size (nm)
CaP(0)	0.22	82
2:1 PEO-complex	0.25	12
4:1 PEO-complex	0.3	9
8:1 PEO-complex	0.36	9
16:1PEO-complex	0.66	8

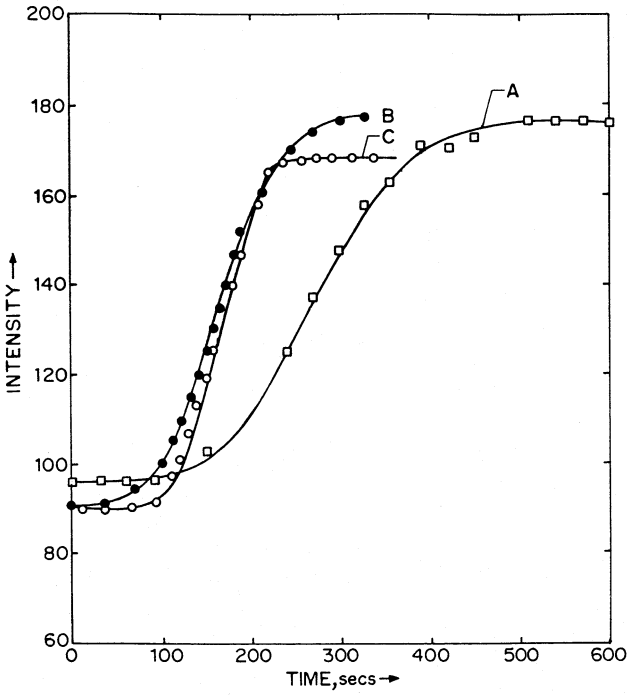

Fig. 7. Isothermal crystallization curves as in Fig. 5 for PP/CaPI and PP/CaPII samples containing 5 wt% filler concentration. Curves A CaPI with 9 nm, curves B and C are for CaPII with 7.5 and 7 nm, respectively.

The comparison of crystallization behaviour of PP/calcium phosphate prepared in PEO alone and that prepared in presence of blends was studied. Fig. 7 corresponds to crystallization curves for 5 wt% nanosize calcium phosphate (8:1 PEO complex) in PP. In this figure, curve A corresponds to PP/CaPI while curves B and C correspond to PP/CaPII with increasing concentration of PVAc of 20 and 40 wt%, respectively. In the presence of blends the induction period decreases much more rapidly and the spherulite size becomes smaller with faster crystallization curves as compared to that observed in PEO alone. The $t_{1/2}$ and growth rates were determined from the curves, which are represented in Table 5 as a function of particle size. As the particle size drops further down due to high amorphous component, i.e. PVAc content, the $t_{1/2}$ value decreases much more quickly and the growth rates increase rapidly for the blends than that containing PEO alone. Thus a definitely high increase in the crystallization rates is observed due to a greater nucleation efficiency of PP in the latter case with a decrease in the ultimate spherulite size as compared to former.

Fig. 8 shows the ultimate spherulite size determined from the crystallization curves of PP/CaPI (PEO alone) as a function of 1/particle size. It is interesting to note that the large particle sized calcium phosphate prepared by conventional method when filled in PP, shows an ultimate spherulite size of nearly 45 μm. However, in presence of nanoparticulate filler in PP, the ultimate spherulite size drops further down and it can be observed that it is lower than 20 μm.

The DSC thermograms were investigated to study the crystallization and melting behaviour of nanofiller dispersed PP composite (curve B) as compared to pure PP (curve A) in Fig. 9. Pure PP (curve A) shows only one exothermic peak whereas the peak form and peak temperature of the nanocomposite (curve B) differs as compared to pure polymer. In presence of nanoparticles of calcium phosphate the crystallization temperature of PP increases from 110 to 114°C and also the width of the crystalline peak narrows down as compared to PP. A remarkable difference can be observed in the endotherm of DSC thermograms. Pure PP shows the heat of fusion (ΔH) of 77.9 J/g whereas the nanofilled PP

Table 5
Dependence of $t_{1/2}$ value and crystallization rates (slope) on particle size for filler synthesized from blend of 8:1 PEO-complex (CaPII)

Composition 5 wt%	$t_{1/2}$	Particle size (nm)
(a) $t_{1/2}$ values		
PEO/PVAc (100:0)	273	9
PEO/PVAc (80:20)	168	7.5
PEO/PVAc (60:40)	162	7
(b) Crystallization rates		
	Rate (μm/s)	Particle size (nm)
PEO/PVAc (100:0)	0.33	9
PEO/PVAc (80:20)	0.55	7.5
PEO/PVAc (60:40)	0.61	7

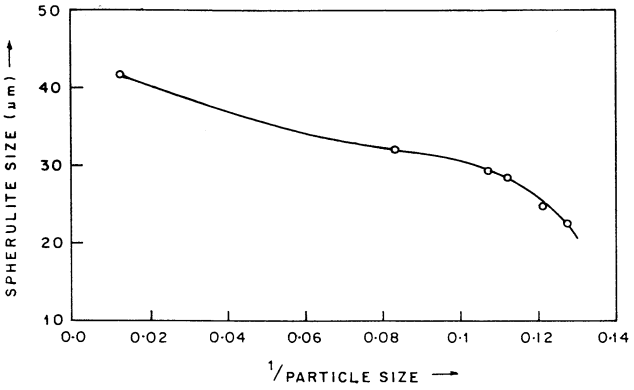

Fig. 8. Ultimate spherulite size as a function of 1/particle size for PP/CaPI samples.

composite shows a broad peak having a ΔH of 132.9 J/g. This dramatic increase in the crystallinity in the endotherm together with increase of crystallization temperature in the exotherm of curve B clearly brings out the strong nucleation

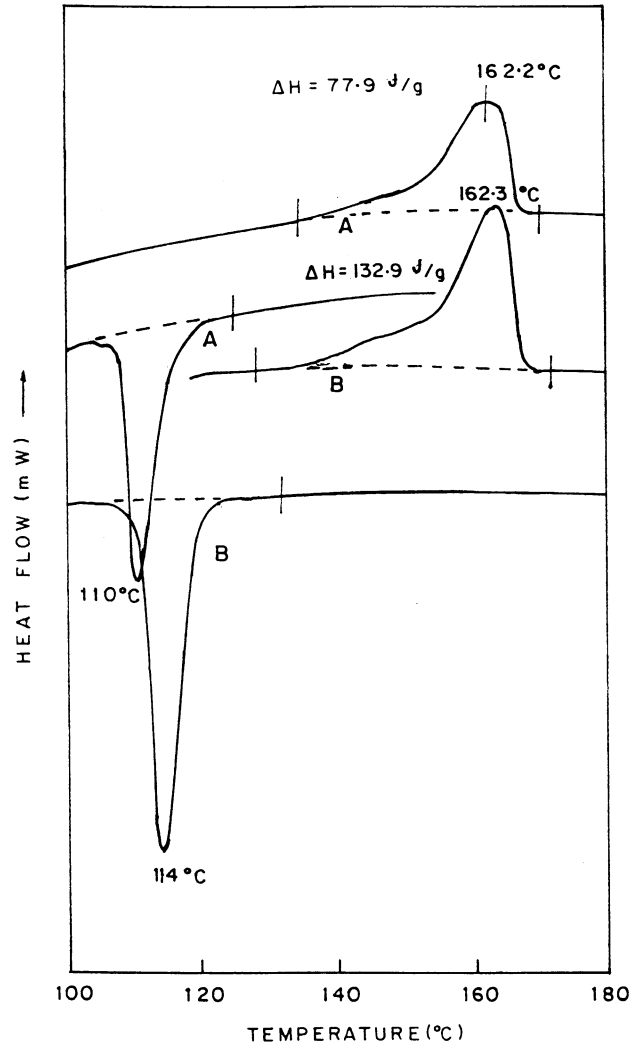

Fig. 9. Comparison of DSC curves for pure PP (curve A) and the nanofilled PP composite (curve B).

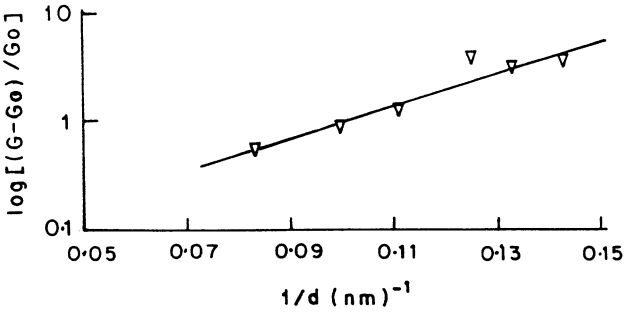

Fig. 10. The effect of particle size on the nucleation efficiency of calcium phosphate in PP. The plot shows the change in crystallization rate with respect to original as a function of (1/*d*) on semi-log scale.

efficiency of nanosize particles on the crystallization of PP leading to faster crystallization rates and decrease of spherulitic dimensions as observed earlier.

A few authors have reported in the past that some fillers such as talc, calcium carbonate, etc. can act as nucleating agents for PP [32–34]. Some also contend that the nucleation is found to be better when the fillers are in fine particulate form. However, the exact dependence of the nucleating efficiency on the particle size has not been reported before. In order to determine this relationship, the increase in crystallization rate (G) due to additive with respect to original without additive $[(G - G_o)/G_o]$ was plotted as function of reciprocal of particle size (1/*d*) in semi-log scale as shown in Fig. 10. From this graph, it is clear that the crystallization (nucleation) rate increases as an inverse exponential power of particle size of the additive, i.e. log $G\alpha(1/d)$ or $G\alpha\exp(1/d)$. Thus, very small size of the particles leads to high nucleation efficiency.

In order to determine the effect of nanosized filler on the optical transparency of PP composite, the UV analysis of isothermally melt crystallized samples containing 2 wt% filler in PP was studied. Fig. 11 shows the graph of extinction coefficient αC as a function of 1/particle size. It is interesting to note that PP/CaP0 shows a high extinction coefficient of 9.4×10^{-3} whereas the calcium phosphate

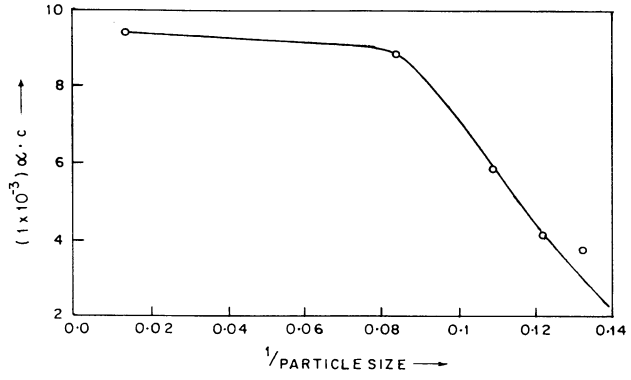

Fig. 11. The extinction parameter (α *C*) as a function of 1/particle size for nanofilled PP/CaPI composite.

prepared by in situ technique (PP/CaPI) shows a decrease of extinction coefficient with increase of 1/particle size (or as the particle size declines). This decrease of extinction coefficient as the particle size reduces further down clearly indicates the decrease of optical density increases the transparency for nanoparticle filled PP. This increase of transparency can be associated with two factors: (a) smaller crystallite size of calcium phosphate at high concentration of PEO, and (b) high crystallization rate of PP in presence of nanoparticles leading to a very small spherulite size.

4. Summary and conclusions

These studies illustrate that nanoparticles of calcium phosphate can be prepared by in situ deposition technique using both PEO and its blend with PVAc. These nanosized particles act as effective nucleating agents for PP compared to that prepared by normal precipitation route. The crystallization behaviour of nanoparticle filled PP exhibits much lower induction period, higher crystallization rates and smaller $t_{1/2}$ value as compared to normal filler. The ultimate spherulite size decreases considerably for these nanoparticulate/PP composites leading to high optical transparency. Interestingly, there are some subtle changes in the growth habit of PP crystallites in these composites: their XRD patterns show changes in the intensities of peaks. The most outstanding part of the present studies is that the nucleating efficiency of these particles as determined by the overall crystallization rate (G) was found to be dependent on the particle size as log $G\alpha(1/d)$. The exact origin for this relationship is not clear at present. Usually one would consider that the nucleation efficiency increases due to increase of surface area as is expected with the reduction in particle size. However, if one considers this as the main cause for increase in nucleation then one has to also take into account the fact that the total surface area is given by $N(4\pi r^2)$, where N is the total number of particles and r is the radius of the particle (assumed to be spherical in shape) which will depend on 1/volume or $[4\pi r^3/3]^{-1}$. This will result in the dependence on $(1/r)$ rather than $\exp(1/r)$, which was observed by us. These differences may arise from the nature of the surface of the nano-particles, which is not exactly the same as that of bulk. Further analysis by X-ray photoelectron spectroscopy (XPS), electron microscopy, etc. may throw some light on the above aspects.

References

[1] Giannelius EP. Adv Mater 1996;8:29.
[2] Smoug D. Mod Plast 1998;2:28.
[3] Kurokawa Y, Yasudo H, Kashiwagi M, Oyo A. J Mater Sci Lett 1997;16(20):1670.
[4] Yano K, Usuki A, Yurauchi T, Kamigaito O. J Polym Sci Part A: Polym Chem 1993;31:2493.
[5] Kawasumi M, Hasegawa N, Kato M, Usuki A, Okada A. Macromolecules 1997;30:6333.

[6] Sanchez C, Babonneau F, Banse F, Doeuff-barboux S, In M, Ribot F. Mater Sci Forum 1994;152(5):313.
[7] Chen Y, Iroh JO. Chem Mater 1999;11:1218.
[8] Usuki A, Kojima Y, Kawasumi M, Okada A, Fukushima Y, Kurauchi T, Kamigaito O. J Mater Res 1993;8:1179.
[9] Wang MS, Pinnavaia TJ. Chem Mater 1994;6:468.
[10] Yang F, Ou Y, Yu Z. J Appl Polym Sci 1998;69:355.
[11] Kiss G. Polym Engng Sci 1987;27:410.
[12] Okada A, Kawasumi M, Usuki A, Kojima Y, Kurauchi T, Kamigaito O. Mater Res Soc Proc 1990;171:45.
[13] Hasegawa N, Kawasumi M, Kato M, Usuki A, Okada A. J Appl Polym Sci 1998;67:87.
[14] Yangchuan K, Chenfen L, Zongneng Q. J Appl Polym Sci 1999;71(7):1139.
[15] Noh MW, Lee DC. Polym Bull 1999;42:619.
[16] Wang Z, Pinnavaia TJ. Chem Mater 1998;10:1820.
[17] Biasci L, Aglietto M, Ruggeri G, Ciardelli F. Polymer 1994;35:3296–304.
[18] Biasci L, Aglietto M, Ruggeri G, D'Alessio A. Polym Adv Technol 1995;6:662.
[19] Dagani R. C and E News 1999;77(23):25.
[20] Yu D. Godovski. Adv Polym Sci 1999;119:79.
[21] Sherman LM. Plast Technol 1999;45(6):53.
[22] Radhakrishnan S. J Cryst Growth 1994;141:437.
[23] Radhakrishnan S. J Cryst Growth 1993;129:191.
[24] Saujanya C, Radhakrishnan S. J Mater Sci 1998;33:1063.
[25] Saujanya C, Ashamol, Radhakrishnan S. Polym Commun 2000;42:2257.
[26] Radhakrishnan S, Khedkar SP. Synth Metals 1996;79:219.
[27] Radhakrishnan S, Unde S. Thin Solid Films 1999;347:229.
[28] Radhakrishnan S, Schultz JM. J Cryst Growth 1992;116:378.
[29] Radhakrishnan S, Mandale AM. Synth Metals 1944;62:217.
[30] Hindeleh AM, Johnson DJ. Polymer 1978;19:29.
[31] Alexander LE. X-ray diffraction methods in polymer science. New York: Wiley, 1969. p. 335.
[32] Takahashi T, Ogata N. J Polym Sci, Part B 1971;9:895.
[33] Last AGM. Macromol Chem 1966;94:30.
[34] Al-Ghazawi M, Sheldon PR. J Polym Sci, Polym Lett 1983;2(5):347.